



## Preparation, characterization and photocatalytic degradation kinetics of Reactive Red dye 198 using N, Fe codoped TiO<sub>2</sub> nanoparticles under visible light

Navneet Kaur<sup>a</sup>, Satwant Kaur<sup>a,b</sup>, Vasundhara Singh<sup>a,\*</sup>

<sup>a</sup>Department of Applied Sciences (Chemistry), PEC University of Technology, Chandigarh 160012, India, Tel. +91 9646765448; email: [navneetpuchem88@gmail.com](mailto:navneetpuchem88@gmail.com) (N. Kaur), Tel. +91 9815620645; email: [shahi.satwant@yahoo.com](mailto:shahi.satwant@yahoo.com) (S. Kaur), Tel. +91 172 2733263; email: [vasun7@yahoo.co.in](mailto:vasun7@yahoo.co.in) (V. Singh)

<sup>b</sup>Department of Chemistry, ASBASJSM College, Bela, Ropar 140001, India

Received 14 August 2014; Accepted 3 March 2015

### ABSTRACT

In this paper, we report the detailed kinetic and mechanistic study using N, Fe codoped TiO<sub>2</sub> for the degradation of Reactive Red dye 198 (RR dye 198) under visible light. The N, Fe codoped TiO<sub>2</sub> was prepared by sol-gel method using urea and ferric nitrate as the dopant source and well characterized by XRD, FTIR, DRS, TEM, XPS, EDX, and BET techniques. The N, Fe codoped TiO<sub>2</sub> nanoparticles were found to be 95.55% anatase and 4.45% rutile phase, with a narrow particle size distribution of 4–7 nm, having band gap of 2.4 eV, surface area of 98.01 m<sup>2</sup> g<sup>-1</sup>, and are cubic in shape. The process conditions for photocatalytic degradation of RR dye 198 using N, Fe codoped TiO<sub>2</sub> under visible light have been optimized by varying operational parameters such as catalyst loading, pH, initial concentration of the substrate, and the effect of electron acceptors have been examined. The addition of H<sub>2</sub>O<sub>2</sub> as a co-oxidant showed an anomalous behavior in the degradation pattern. The degradation followed first-order kinetics with  $r_0$  of 3.036 mg L<sup>-1</sup> min<sup>-1</sup> at natural pH and obeyed the Langmuir-Hinshelwood model. The mechanism of degradation has been investigated with the help of radical quenchers. The GC-MS analysis of the residue after degradation depicted the degradation pattern of the dye under optimized conditions.

*Keywords:* Photocatalytic degradation; Kinetics; Mechanistic study; Reactive Red dye 198

### 1. Introduction

Various physical, chemical, and biological pre-treatment and post-treatment techniques have been developed over the last two decades to remove color from dye-contaminated wastewaters in order to meet environmental regulatory requirement, but these treatment methods have their own disadvantages.

These methods do not bring down the pollution parameters to the satisfactory level, and simply transfer the pollutants from one medium to another. Merely transferring toxic materials from one medium to another is not a long-term solution to the problem of hazardous waste loading on the environment. The recent developments in water decontamination processes are concerned with the oxidation of these bio-recalcitrant organic compounds. These methods rely on the formation of highly reactive chemical

\*Corresponding author.

species that degrade more number of recalcitrant molecules into biodegradable compounds and are called advanced oxidation processes (AOPs).

In AOPs, the efficient utilization of solar energy is one of the major goals that will influence the future technological applications [1–3]. Among the various materials being developed for photocatalytic applications, TiO<sub>2</sub> remains the most promising because of its high efficiency, low cost, chemical inertness, and photostability [4,5]. However, the major drawback of TiO<sub>2</sub> lies in their ineffective use of visible light as irradiation source because of the large band gap of anatase TiO<sub>2</sub> (3.2 eV). Due to this, it can absorb and is excited by only UV light having  $\lambda$  less than 387 nm, which occupies only 4.6% of global solar radiation.

Many studies have been devoted to solve this problem via doping of TiO<sub>2</sub> to change its electronic structure [6]. Asahi et al. [7,8] successfully synthesized N-doped TiO<sub>2</sub> by heat treatment of TiO<sub>2</sub> in N<sub>2</sub> or NH<sub>3</sub> atmosphere, which showed high activity under visible light irradiation. Besides nitrogen doping, other anions such as C, S, and F were also found to be effective to enhance the photocatalytic activity under visible light irradiation [9–14]. However, non-metal doping brings in the serious problem of massive charge carrier re-combination which largely limits the photoactivity of doped TiO<sub>2</sub> under visible light.

Doping with metal cations is also a typical approach to extend the spectral response of TiO<sub>2</sub> to the visible light region by providing defect states in the band gap. Metal ions such as Fe, Cr, Co, Mo, V to mention a few have been reported to be effective in enhancing visible light photocatalytic activity of TiO<sub>2</sub>. Choi et al. [15] have reported that TiO<sub>2</sub>, doped with 21 different metal ions prepared by sol–gel method, exhibited various colors depending on the ion used.

Recently, codoping with metals and non-metals has also been widely investigated [16–20]. To study the synergistic effect of both metal and non-metal ions which can extend the absorption edge of TiO<sub>2</sub> into visible light range more efficiently, various combinations of metal and non-metal have been reported in literature [21,22]. Among metal and non-metal codoped TiO<sub>2</sub> catalysts, N, Fe codoped TiO<sub>2</sub> is considered to be an effective combination [23].

Till date, the focus of research in this area has been mainly toward developing new synthetic methods for doping of TiO<sub>2</sub> with metals, non-metals, and combination of both. However, the detailed kinetic and mechanistic study for degradation of reactive dyes using metal and non-metal codoped TiO<sub>2</sub> has not been reported in literature. In continuation to our work in the area of photocatalytic degradation of reactive dyes [24] and our efforts to harness the solar light, in this

paper we report the detailed kinetic and mechanistic study using N, Fe codoped TiO<sub>2</sub> under visible light for degradation of RR dye 198 for optimization of reaction parameters and evaluation of the degradation pattern.

## 2. Materials and methods

### 2.1. Materials

- Sample: Commercially available Reactive Red dye 198 (RR dye 198) was gifted from a Textile Industry, Nahar Fabrics, Derabassi, Punjab, India and was used as such without any purification.
- Reagents and chemicals: Hydrogen peroxide (30% v/v solution) was used as an oxidant. Hydrochloric acid and sodium hydroxide (Merck, India) were used to adjust pH. The radical quenchers used were sodium azide (NaN<sub>3</sub>), 1,4-diazobicyclo [2,2,2] octane (DABCO), 1,4-benzoquinone (Sigma Aldrich).

### 2.2. Preparation method of codoped TiO<sub>2</sub> catalyst

N, Fe codoped TiO<sub>2</sub> powder was synthesized by sol-gel method. Firstly, tetrabutyl titanate (10 ml) and acetic acid (10 ml) were added in 50 ml absolute ethanol (solution A). Secondly, 0.1765 g of ferric nitrate [Fe (NO<sub>3</sub>)<sub>3</sub>·3H<sub>2</sub>O], 3.6 g urea, 5 ml acetic acid, and 6.25 ml distilled water were added in 25 ml absolute ethanol (solution B). The solution B was added dropwise into solution A with vigorous magnetic agitation. The obtained mixture was stirred for 3 h, and then kept at room temperature in air for 24 h to form a homogeneous gel. The as-prepared gel was dried at 80 °C in the oven, then it was porphyzied into powder and annealed at 500 °C at a rate of 3 °C min<sup>-1</sup> in a programmable furnace for 3 h. Finally, a light yellow powder was obtained. The material was characterized by XRD, FTIR, DRS, TEM, XPS, EDX, and BET techniques.

### 2.3. Characterization

The XRD patterns (Fig. 1) of N, Fe codoped TiO<sub>2</sub> catalyst indicates that the structure consists of anatase and rutile phases while undoped TiO<sub>2</sub> exhibits the pure anatase phase. The anatase and rutile phase contents of the codoped TiO<sub>2</sub> were calculated by analyzing the intensities of anatase 101 peak at

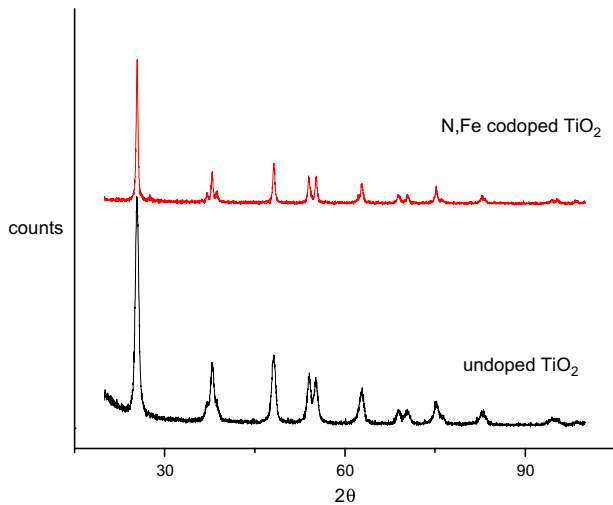


Fig. 1. XRD pattern of N, Fe codoped TiO<sub>2</sub>.

$2\theta = 25.5^\circ$  and rutile 110 peak at  $2\theta = 27.5^\circ$ . The anatase fraction ( $F_A$ ) was found by the following equation:

$$F_A = 100 - \frac{1}{1 + \frac{0.8I_A}{I_R}} \cdot 100 \quad (1)$$

where  $I_A$  is the intensity of the 101 peak of anatase and  $I_R$  is the intensity of the 110 peak of rutile. From this equation, anatase phase has been found to be 95.55% and rutile phase was 4.45% in the N, Fe codoped TiO<sub>2</sub>.

The average crystallite size of the sample has been estimated using Debye–Scherer equation:

$$d = \frac{0.89\lambda}{\beta \cos\theta} \quad (2)$$

where  $d$  represents the crystallite size,  $\lambda$  is the wavelength of incident X-ray,  $\beta$  is the full width at half maximum of diffraction formula, and  $\theta$  represents the scattering angle. The mean grain size of the N, Fe codoped TiO<sub>2</sub> has been estimated as 4 nm by Scherer's equation.

As shown in the TEM image (Fig. 2) of the powder, most of the particles were of approximately spherical morphology, and the grain size was found to be in the range of 4–7 nm, which is in good agreement with that obtained from the Scherer's method.

Fig. 3 shows the particle size distribution of N, Fe codoped TiO<sub>2</sub>. The average particle size was 252.5 nm, larger than the result of XRD and TEM analysis. This

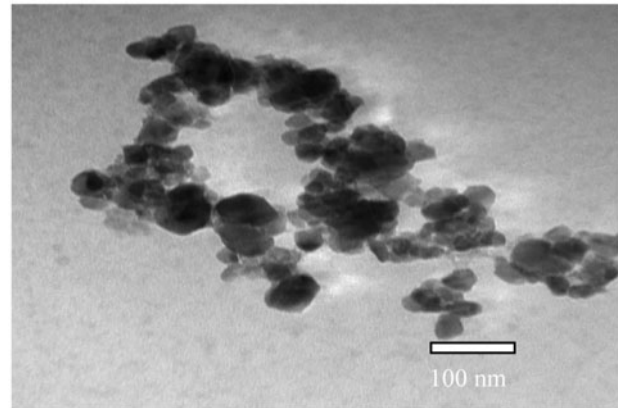


Fig. 2. TEM image of N, Fe codoped TiO<sub>2</sub>.

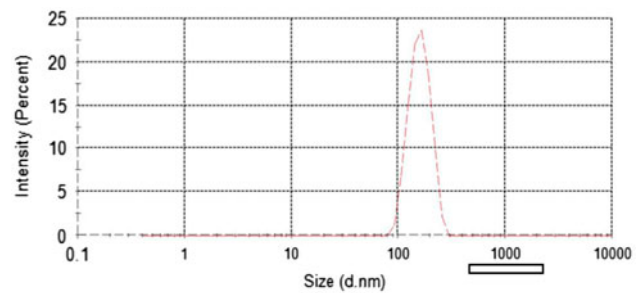


Fig. 3. Particle size distribution of N, Fe codoped TiO<sub>2</sub>.

attributes to the agglomeration of the powder at the concentration at which analysis has been done.

The specific surface area of codoped TiO<sub>2</sub> was measured and found to be 98.01 m<sup>2</sup> g<sup>-1</sup> by BET method. The physicochemical properties have been summarized in Table 1.

Fig. 4 shows FT-IR spectra of the photocatalyst wherein the peak at 3,400 cm<sup>-1</sup> (stretching vibration) and the peak around 1,640 cm<sup>-1</sup> (bending vibration) for the sample corresponds to the adsorbed water molecules over the sample. The peak at 742 cm<sup>-1</sup> was due to the stretching vibration of Ti–O bond. The peaks at around 1,450, 1,230, and 1,090 cm<sup>-1</sup> can be attributed to the nitrogen atoms embedded in the TiO<sub>2</sub> network.

The UV–vis diffuse reflectance spectra (Fig. 5) showed that the absorption edge of the N, Fe codoped TiO<sub>2</sub> was red shifted up to 700 nm which means that the light absorption range expanded to the visible region. The band gap energy of N, Fe codoped TiO<sub>2</sub> was determined from the Tauc relationship and was found to be 2.4 eV as shown in Fig. 5.

Fig. 6 shows the XPS spectra of N 1s at 399.8 eV which can be attributed to N–O bonds. This indicates

Table 1  
Physicochemical properties of N, Fe codoped TiO<sub>2</sub> catalyst

Surface area (m <sup>2</sup> g <sup>-1</sup> )	Pore diameter (Å)	Band gap (eV)	Phase (%)	Particle size (nm)	FTIR (cm <sup>-1</sup> )
98.01	65.11	2.4	95.55 anatase, 4.45 rutile	XRD-4 TEM-4-7	3,400, 1,640—H <sub>2</sub> O stretching, bending vibration 742—stretching vibration of Ti–O 1,450, 1,230, 1,090—N–Ti–O

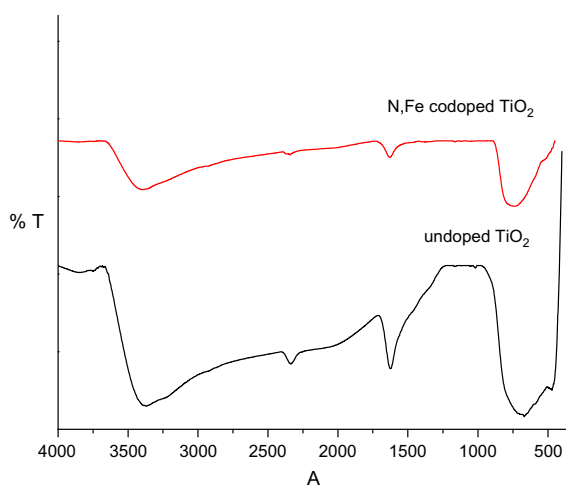


Fig. 4. FTIR spectra of N, Fe codoped TiO<sub>2</sub>.

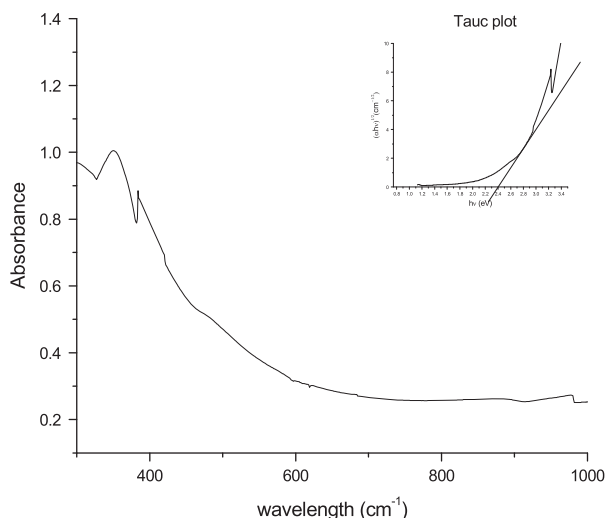


Fig. 5. UV–vis DRS and Tauc plot of N, Fe codoped TiO<sub>2</sub>.

that the nitrogen atoms were weaved into the crystal structure of titania, which was further confirmed by DRS analysis. The binding energies of the peaks located at 723.5 and 709.7 eV in XPS spectra of Fe 2p

indicated the existence of Fe–O bond on the surface of the sample.

The chemical composition of the sample was determined by energy-dispersive spectroscopy (Fig. 7). The intense peak is assigned to the bulk TiO<sub>2</sub>. The peaks due to Fe are clearly distinct at 0.5, 6.5, and 7.0 keV. The peaks due to N do not come up, which may be due to the low doping content.

## 2.4. Experimental procedure and techniques

### 2.4.1. Photodegradation experiments

Photocatalytic experiments were performed with 200 ml of dye solution in an immersion well type reactor. The experiment was carried out under visible light irradiation using 100 W halogen lamp with the circulation of 2 M NaNO<sub>2</sub> solution for absorption of any irradiation below 400 nm and vigorous bubbling was done to increase dissolved oxygen concentration. The solution was stirred continuously. An aliquot of 5 ml was taken from the reactor at regular intervals of time with a syringe. The suspension was centrifuged for five min at 4,000 rpm and subsequently filtered through a Millipore filter (pore size 0.45 μm) to remove TiO<sub>2</sub> particles. These samples were analyzed at λ<sub>max</sub> = 515 nm by Perkin-Elmer Lambda 35 UV–vis spectrophotometer.

### 2.4.2. Adsorption experiments

The adsorption studies were performed using an aqueous solution of dye. For this purpose, dye solution (50 ml) of different concentrations of 10, 20, 30, 40, and 50 ppm were kept in dark for 2 h in the presence of 100 mg of N, Fe codoped TiO<sub>2</sub> photocatalyst at room temperature. The dye concentration (C<sub>e</sub>) in the supernatant liquid was measured spectrophotometrically. The amount of dye adsorbed (q<sub>e</sub>) onto the surface of TiO<sub>2</sub> photocatalyst was estimated by subtracting the value of equilibrium dye concentration (C<sub>e</sub>) from the initial dye concentration (C<sub>0</sub>).

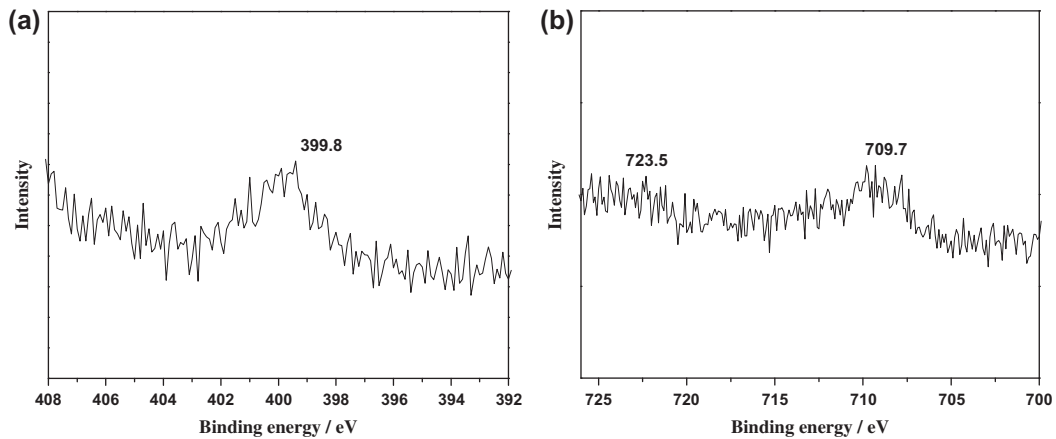


Fig. 6. XPS spectra of N, Fe codoped TiO<sub>2</sub> (a) N 1s (b) Fe 2p.

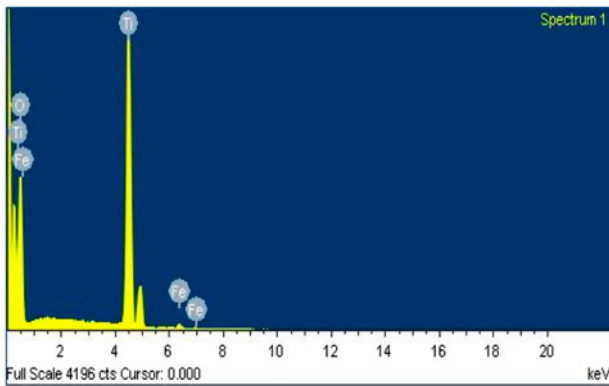


Fig. 7. EDX spectra of N, Fe codoped TiO<sub>2</sub>.

### 3. Kinetic studies

#### 3.1. Kinetics of adsorption

The adsorption tests were carried out under dark conditions as per the procedure mentioned above. Fig. 8(a) shows that adsorption of dye from aqueous solution strongly depends on the pH of solution.

The equilibrium constants were determined by fitting the experimental data to the Langmuir equation (Eq. (3)) to describe the adsorption of the dye on the homogeneous surface of N, Fe codoped TiO<sub>2</sub>

$$q_e = \frac{q_m b C_e}{1 + b C_e} \quad (3)$$

$$K_a = q_m b \quad (4)$$

where  $q_m$  is the maximum amount of dye adsorbed forming a complete monolayer,  $b$  is the equilibrium parameter,  $C_e$  is the concentration of dye in aqueous

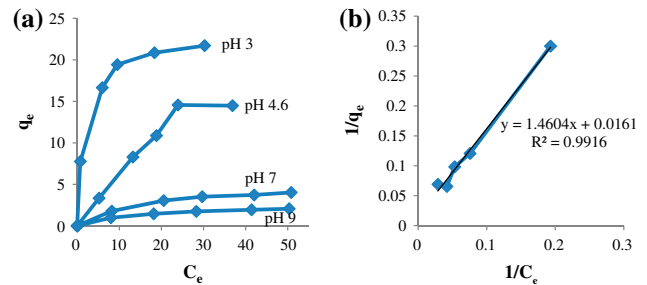


Fig. 8. (a) Adsorption isotherms of RR dye 198 on N, Fe codoped TiO<sub>2</sub> surface at different initial pH (b) Plot of  $1/q_e$  vs.  $1/C_e$  for adsorption of RR dye 198, catalyst = 100 mg, pH 4.6.

solution, and  $q_e$  is the concentration of dye on the solid. The plot of  $1/q_e$  vs.  $1/C_e$  has been found to be linear in each case as shown in Fig. 8(b) for natural pH 4.6. The Langmuir equilibrium constants as per Eq. (4) are shown in Table 2.

#### 3.2. Kinetics of degradation experiments

The photocatalytic degradation of RR dye 198 containing N, Fe codoped TiO<sub>2</sub> obeys pseudo-first-order

Table 2  
Langmuir equilibrium constants for the adsorption of RR dye 198 on N, Fe codoped TiO<sub>2</sub> in dark

pH	$K_a$ (g L <sup>-1</sup> )
3	15.87
4.6	0.6851
5	0.3283
7	0.1992

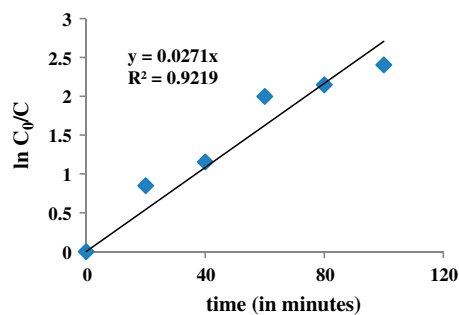


Fig. 9. Kinetics of photocatalytic degradation of RR dye 198;  $C_0 = 10$  ppm, pH 4.6, catalyst =  $1.2 \text{ g L}^{-1}$ .

kinetics. At low initial dye concentration, the rate expression is given by

$$\frac{-dC}{dt} = k'[C] \quad (5)$$

where  $k'$  is the pseudo-first-order rate constant.

The influence of initial concentration of the solute on the degradation rate of RR dye 198 can be described by a pseudo-first-order kinetics, which is given in terms of the Langmuir–Hinshelwood model Eq. (6), modified for heterogeneous catalytic reactions:

$$R_0 = -\frac{dC}{dt} = \frac{k_v K_e C_0}{1 + K_e C_0} \quad (6)$$

where  $k_v$  reflects the limiting rate of the reaction at maximum coverage under the given experimental conditions.  $K_e$  represents the equilibrium constant for adsorption of dye on to illuminated  $\text{TiO}_2$ . In Eq. (6),  $k_v$  represents the apparent rate constant because it is also dependent on the source of visible light and the radiation field inside a photocatalytic reactor.

The kinetics of photodegradation as a function of pH has also been described using Langmuir–Hinshelwood model Eq. (6). The photocatalytic degradation of RR dye 198 follows first-order kinetics as shown in Fig. 9 depicting a linear fit between  $\ln(C_0/C)$  and irradiation time.

## 4. Results and discussion

### 4.1. Effect of catalyst loading

The effect of concentration of the photocatalyst on the degradation rate of RR dye 198 has been investigated by employing different concentrations of N, Fe codoped  $\text{TiO}_2$  varying from  $0.9$  to  $3 \text{ g L}^{-1}$  under visible light. It was observed that initial rate ( $r_0$ ) increased

with increase in photocatalyst concentration, wherein the most appreciable change of  $r_0$  came when photocatalyst concentration increases from  $0.9$  to  $1.2 \text{ g L}^{-1}$  beyond which up to  $3 \text{ g L}^{-1}$  there was no appreciable change as shown in Table 3. Therefore, the optimum catalyst concentration chosen for the degradation was  $1.2 \text{ g L}^{-1}$ . This can be attributed to the fact that the number of photons absorbed and the number of dye molecules adsorbed are known to increase with the increase in catalyst concentration, thereby enhancing the rate of degradation. Beyond a minimum catalyst concentration, the rate does not increase to appreciable extent which is because of the opacity and screening effect of excess catalyst that acts as a shield to hinder the light penetration.

Based on the empirical relationship,  $r_0 \propto [\text{TiO}_2]^n [\text{dye}]$ , Fig. 10 depicts the dependence of  $\text{TiO}_2$  concentration on the initial decolorization rate when catalyst concentration is less than  $1.2 \text{ g L}^{-1}$  [25].

### 4.2. Effect of initial substrate concentration

The effect of initial concentration of dye solution on the degradation rate of RR dye 198 has been investigated by varying the dye concentrations from  $10$  to  $40 \text{ mg L}^{-1}$  in the presence of  $1.2 \text{ g L}^{-1}$  of N, Fe codoped  $\text{TiO}_2$  under visible light as shown in Fig. 11. It has observed that for the same time period, the photo-degradation process is effective at low concentration as degradation decreases from  $94$  to  $70\%$  when initial substrate concentration increases from  $10$  to  $40$  ppm. This can be explained by the adsorption behavior of dye in which the concentration of unadsorbed dye in solution increases leading to lesser penetration of light through the solution onto the surface of catalyst. In spite of this, as the concentration of dye increases, the requirement of reactive species ( $\cdot\text{OH}$  and  $\cdot\text{O}_2^-$ ) needed for the degradation also increases. However, the formation of  $\cdot\text{OH}$  and  $\cdot\text{O}_2^-$  on the catalyst surface remains constant for a given light

Table 3

Effect of N, Fe codoped  $\text{TiO}_2$  loading on the degradation rate during the photocatalytic oxidation ( $C_0 = 30 \text{ mg L}^{-1}$ , pH 4.6)

N, Fe codoped $\text{TiO}_2$ ( $\text{g L}^{-1}$ )	$r_0$ ( $\text{mg L}^{-1} \text{ min}^{-1}$ )
0.9	2.675
1.2	3.036
1.5	3.097
1.8	3.127
2.1	3.329
3	3.625

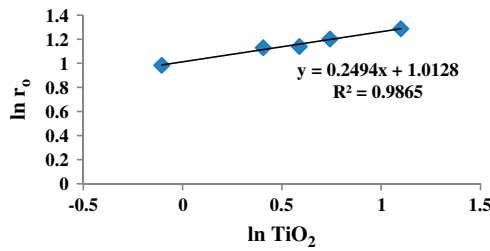


Fig. 10. Relationship between  $r_0$  and the amount of catalyst; pH 4.6,  $C_0 = 30$  ppm.

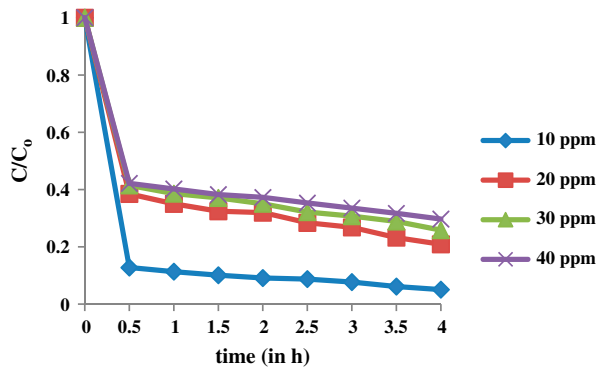


Fig. 11. Kinetics of photodegradation of RR dye 198 at different initial concentrations.

intensity, catalyst amount, and duration of irradiation that decreases the degradation rate at higher concentration [26]. In addition, slow diffusion of the generated intermediates from the catalyst surface can result in the deactivation of active sites of the photocatalyst, and, consequently, a reduction in the degradation rate.

The influence of the initial concentration of solute on the degradation rate of most of the organic compounds can be described by a pseudo-first-order kinetics in terms of Langmuir–Hinshelwood equation (Eq. (6)) modified to accommodate reactions occurring at a solid–liquid interface. A linear expression can be obtained by plotting the reciprocal of initial rate against the reciprocal of initial concentration as shown in Fig. 12.

#### 4.3. Effect of initial pH of the solution

Employing  $1.2 \text{ g L}^{-1}$  N, Fe codoped  $\text{TiO}_2$  as a photocatalyst, the degradation of RR dye 198 was studied in the pH range between 3 and 9 as shown in Fig. 13. At pH 3, complete adsorption of dye takes place while at pH 9, negligible adsorption takes place resulting in decreased rate of degradation of the dye. It was found that maximum degradation of the dye

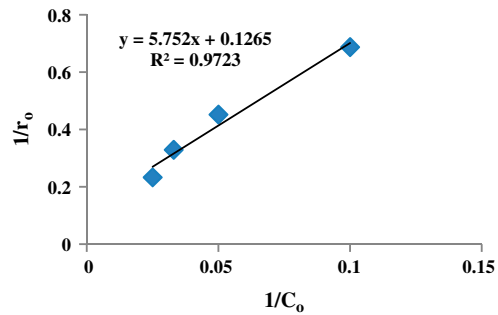


Fig. 12. Representation of Langmuir–Hinshelwood equation: pH = normal,  $[\text{TiO}_2] = 1.2 \text{ g L}^{-1}$ .

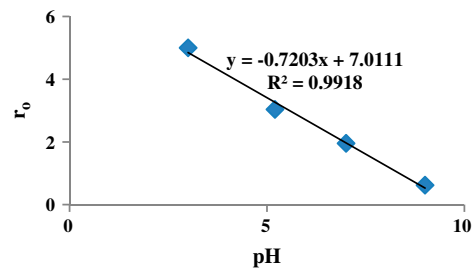


Fig. 13. Effect of pH on initial rate of degradation of RR dye 198:  $[\text{TiO}_2] = 1.2 \text{ g L}^{-1}$ ,  $C_0 = 30$  ppm.

took place at the natural pH of 4.6. This can be accounted to the effective adsorption and generation of reactive radicals for efficient degradation because N, Fe codoped  $\text{TiO}_2$  acquires a positive charge in acidic media. Since the dye has negatively charged sulfonate group in its structure, the acidic solution favors the adsorption of the dye onto photocatalyst surface; thus, the photodegradation efficiency increases [27].

The results are summarized by the  $K_e$  and  $k_v$  values of the Langmuir–Hinshelwood equation as shown in Table 4.

#### 4.4. Effect of $\text{H}_2\text{O}_2$ addition

The addition of  $\text{H}_2\text{O}_2$  increases the concentration of  $\cdot\text{OH}$  radicals and thereby is known to enhance the rate of degradation of dye [28]. Fig. 14 shows the change in degradation rate by varying the amount of  $\text{H}_2\text{O}_2$  concentration at natural pH and at optimum catalyst loading. It was observed that the addition of  $\text{H}_2\text{O}_2$  decreases the degradation rate of the RR dye 198. This is an unusual result indicating a possibly different mechanism for degradation at the surface of N, Fe codoped  $\text{TiO}_2$  wherein the excess hydroxyl radicals provided by the addition of  $\text{H}_2\text{O}_2$  are not effective in

Table 4  
Langmuir–Hinshelwood constants for the degradation of RR dye 198 at different pH values

pH	$K_e$ (L mg <sup>-1</sup> )	$k_v$ (min <sup>-1</sup> )
4.6	0.02191	7.9365
7	0.02674	4.1323
9	0.05445	1.0163

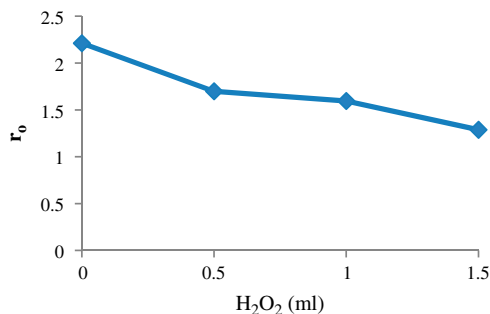


Fig. 14. Effect of H<sub>2</sub>O<sub>2</sub> concentration on the initial rate at C<sub>0</sub> = 20 ppm, pH = natural, catalyst = 1.2 g L<sup>-1</sup>.

enhancing the degradation. Rather, it decreases the effect of the other oxidative species, particularly the superoxide radical which has been found to be active

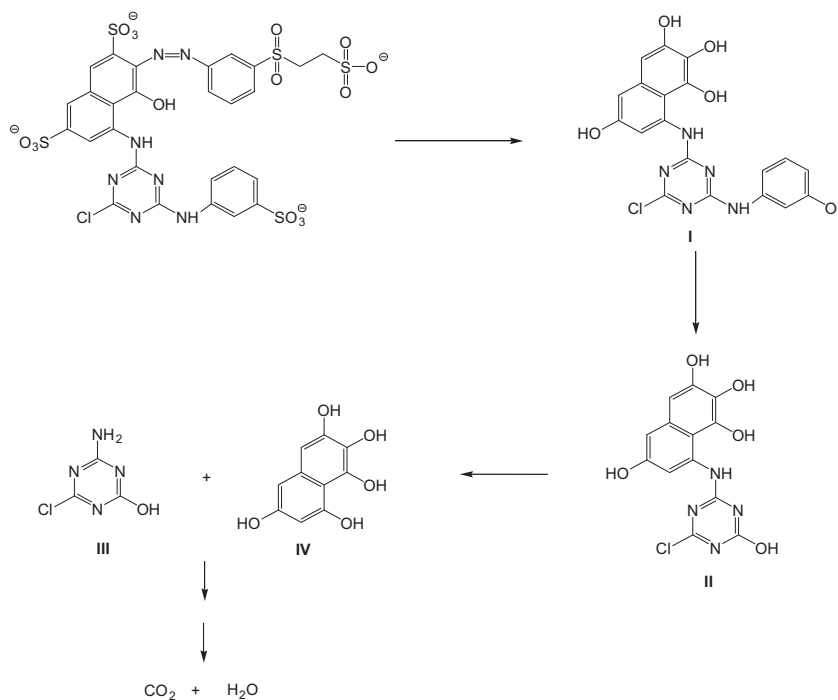


Fig. 16. Reaction pathway of photocatalytic degradation of RR dye 198 under visible light.

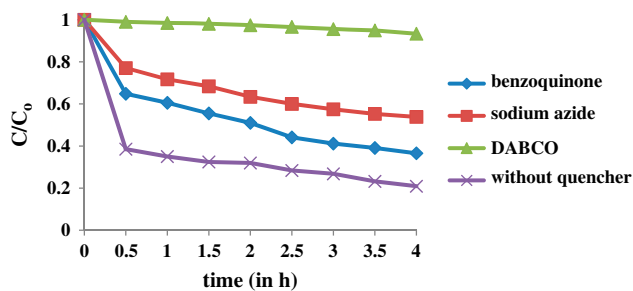


Fig. 15. The effect of radical quenchers on the photocatalytic degradation rate C<sub>0</sub> = 20 ppm, N, Fe codoped TiO<sub>2</sub> = 0.24 g/200 ml, quencher = 0.02 g/200 ml.

in the degradation process as indicated during the mechanistic studies by the addition of various radical quenchers.

#### 4.5. Mechanism of degradation of RR198 under visible light

##### 4.5.1. Effect of radical quenchers

To understand the role of various oxidative species involved in the degradation process, few radical quenchers have been used. Three different compounds, NaN<sub>3</sub>, DABCO, and 1,4-benzoquinone were added in three individual experiments as shown in Fig. 15 and the suspension was irradiated under

identical conditions. It has observed that in the presence of DABCO, which is a singlet oxygen quencher, photobleaching of RR dye 198 is completely suppressed, indicating that the singlet oxygen is an active oxidative intermediate. The inhibiting effect of  $\text{NaN}_3$ , which is an  $^1\text{O}_2$  quencher but may also interact with  $\cdot\text{OH}$  radical, becomes significant after 1 h indicating the delayed formation of singlet oxygen (and possibly hydroxyl radical) species. Similar results were obtained after addition of 1,4-benzoquinone, which is known to be a superoxide quencher.

#### 4.5.2. GC–MS analysis of degradation intermediates

An attempt was also made to identify the intermediate products formed in the photocatalytic degradation of the dye after decolorization through GC–MS analysis. The GCMS analysis of the solution after complete decolorization in 12 h showed the formation of the intermediates as depicted in Fig. 16. The cleavage of the azo bond results in formation of intermediate I, which on further oxidation by singlet oxygen and other reactive species, results in formation of intermediates II, III, IV as confirmed by MS fragmentation pattern. These benign intermediates can be further mineralized to form  $\text{CO}_2$  and  $\text{H}_2\text{O}$ .

#### 4.6. Photodegradation by solar irradiation

After optimizing the process parameters for the degradation of dye under artificially simulated visible light in the lab, the degradation of the RR dye 198 was also studied under sunlight in a shallow pond slurry reactor. It was observed that degradation of dye under sunlight was 100% in 3 h as compared to 94% degradation under artificial visible light in the same duration of time as shown in Fig. 17. The enhanced

degradation under sunlight is due to the combined effect of UV and visible light.

## 5. Conclusion

In this paper, the process optimization with extensive kinetic and mechanistic detail for the degradation of RR dye 198, a reactive dye, using a synthesized visible light active N, Fe codoped  $\text{TiO}_2$  catalyst has been presented. The rate of photodegradation was found to be dependent on pH, initial substrate concentration, catalyst loading, and  $\text{H}_2\text{O}_2$  addition. An unusual result was observed as the rate of degradation decreases with the addition of  $\text{H}_2\text{O}_2$ . The photodegradation follows first-order kinetics and obeys the Langmuir–Hinshelwood model. The most active oxidative species has been found to be the superoxide radical and the major degradation product formed by the cleavage of the chromophoric group has been indicated by GC–MS analysis. This study is significant for the implementation of metal, non-metal doped  $\text{TiO}_2$  for harnessing the visible light component for solar detoxification of industrial wastewaters mainly from textile industry.

## Acknowledgments

The authors are grateful to PEC University of Technology, Chandigarh for the financial support and for providing the various facilities.

## References

- [1] A. Fujishima, K. Honda, Electrochemical photolysis of water at a semiconductor electrode, *Nature* 238 (1972) 37–38.
- [2] S.U.M. Khan, J. Akikusa, Photoelectrochemical splitting of water at nanocrystalline  $n\text{-Fe}_2\text{O}_3$  thin-film electrodes, *J. Phys. Chem. B* 103 (1999) 7184–7189.
- [3] S. Licht, B. Wang, S. Mukerji, T. Soga, M. Umeno, H. Tributsch, Efficient solar water splitting, exemplified by  $\text{RuO}_2$ -catalyzed  $\text{AlGaAs/Si}$  photoelectrolysis, *J. Phys. Chem. B* 104 (2000) 8920–8924.
- [4] K. Hashimoto, H. Irie, A. Fujishima,  $\text{TiO}_2$  photocatalysis: A historical overview and future prospects, *Jpn. J. Appl. Phys.* 44 (2005) 8269–8285.
- [5] A.L. Linsebigler, G. Lu, J.T. Yates, Photocatalysis on  $\text{TiO}_2$  surfaces: Principles, mechanisms, and selected results, *Chem. Rev.* 95 (1995) 735–758.
- [6] M. Pelaez, N.T. Nolan, S.C. Pillai, M.K. Seery, P. Falaras, A.G. Kontos, P.S.M. Dunlop, J.W.J. Hamilton, J.A. Byrne, K. O’Shea, M.H. Entezari, D.D. Dionysiou, A review on the visible light active titanium dioxide photocatalysts for environmental applications, *Appl. Catal., B* 125 (2012) 331–349.

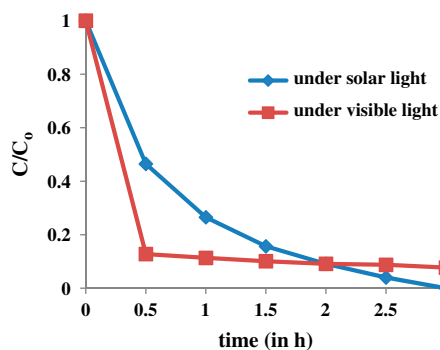


Fig. 17. Photocatalytic degradation of RR dye 198 under sunlight;  $C_0 = 10$  ppm, catalyst =  $1.2 \text{ g L}^{-1}$ .

- [7] T. Morikawa, R. Asahi, T. Ohwaki, K. Aoki, Y. Taga, Band-gap narrowing of titanium dioxide by nitrogen doping, *Jpn. J. Appl. Phys.* 40 (2001) L561–L563.
- [8] R. Asahi, T. Morikawa, T. Ohwaki, K. Aoki, Y. Taga, Visible-light photocatalysis in nitrogen-doped titanium oxides, *Science* 293 (2001) 269–271.
- [9] Q. Zhang, J. Wang, S. Yin, T. Sato, F. Saito, Synthesis of a visible-light active  $\text{TiO}_{2-x}\text{S}_x$  photocatalyst by means of mechanochemical doping, *J. Am. Ceram. Soc.* 87 (2004) 1161–1163.
- [10] D. Huang, S. Liao, J. Liu, Z. Dang, L. Petrik, Preparation of visible-light responsive N-F-codoped  $\text{TiO}_2$  photocatalyst by a sol-gel-solvothermal method, *J. Photochem. Photobiol., A* 184 (2006) 282–288.
- [11] J. Xu, J. Li, W. Dai, Y. Cao, H. Li, K. Fan, Simple fabrication of twist-like helix N, S-codoped titania photocatalyst with visible-light response, *Appl. Catal. B Environ.* 79 (2008) 72–80.
- [12] S.U.M. Khan, M. Al-Shahry, W.B. Ingler Jr., Efficient photochemical water splitting by a chemically modified  $n\text{-TiO}_2$ , *Science* 297 (2002) 2243–2245.
- [13] T. Umebayashi, T. Yamaki, S. Tanaka, K. Asai, Visible light-induced degradation of methylene blue on S-doped  $\text{TiO}_2$ , *Chem. Lett.* 32 (2003) 330–331.
- [14] J.C. Yu, J.G. Yu, W.K. Ho, Z.T. Jiang, L.Z. Zhang, Effects of  $\text{F}^-$  doping on the photocatalytic activity and microstructures of nanocrystalline  $\text{TiO}_2$  powders, *Chem. Mater.* 14 (2002) 3808–3816.
- [15] W. Choi, A. Termin, M.R. Hoffmann, The role of metal ion dopants in quantum-sized  $\text{TiO}_2$ : Correlation between photoreactivity and charge carrier recombination dynamics, *J. Phys. Chem.* 98 (1994) 13669–13679.
- [16] Y. Cong, J.L. Zhang, F. Chen, M. Anpo, D.N. He, Preparation, photocatalytic activity, and mechanism of nano- $\text{TiO}_2$  co-doped with nitrogen and iron (III), *J. Phys. Chem. C* 111 (2007) 10618–10623.
- [17] L. Jia, C. Wu, S. Han, N. Yao, Y.Y. Li, Z.B. Li, B. Chi, J. Pu, L. Jian, Theoretical study on the electronic and optical properties of (N, Fe)-codoped anatase  $\text{TiO}_2$  photocatalyst, *J. Alloys Compd.* 509 (2011) 6067–6071.
- [18] K. Song, J. Zhou, J. Bao, Photocatalytic activity of (copper, nitrogen)-codoped titanium dioxide nanoparticles, *J. Am. Ceram. Soc.* 91 (2008) 1369–1371.
- [19] X. Li, Z.M. Chen, Y.C. Shi, Y.Y. Liu, Preparation of N, Fe co-doped  $\text{TiO}_2$  with visible light response, *Powder Technol.* 207 (2011) 165–169.
- [20] K.S. Rane, R. Mhalsiker, S. Yin, T. Sato, K. Cho, E. Dunbar, P. Biswas, Visible light-sensitive yellow  $\text{TiO}_{2-x}\text{N}_x$  and Fe-N co-doped  $\text{Ti}_{1-y}\text{Fe}_y\text{O}_{2-x}\text{N}_x$  anatase photocatalysts, *J. Solid State Chem.* 179 (2006) 3033–3044.
- [21] S. Song, J. Tu, L. Xu, X. Xu, Z. He, J. Qiu, J. Ni, Preparation of a titanium dioxide photocatalyst codoped with cerium and iodine and its performance in the degradation of oxalic acid, *Chemosphere* 73 (2008) 1401–1406.
- [22] A.T. Kuvarega, R.W.M. Krause, B.B. Mamba, Nitrogen/palladium-codoped  $\text{TiO}_2$  for efficient visible light photocatalytic dye degradation, *J. Phys. Chem. C* 115 (2011) 22110–22120.
- [23] Y. Su, Y. Xiao, Y. Li, Y. Du, Y. Zhang, Preparation, photocatalytic performance and electronic structures of visible-light-driven Fe-N-codoped  $\text{TiO}_2$  nanoparticles, *Mater. Chem. Phys.* 126 (2011) 761–768.
- [24] S. Kaur, V. Singh, Visible light induced sonophotocatalytic degradation of Reactive Red dye 198 using dye sensitized  $\text{TiO}_2$ , *Ultrason. Sonochem.* 14 (2007) 531–537.
- [25] C. Galindo, P. Jacques, A. Kalt, Photooxidation of the phenylazonaphthol AO20 on  $\text{TiO}_2$ : Kinetic and mechanistic investigations, *Chemosphere* 45 (2001) 997–1005.
- [26] W. Bahnemann, M. Muneer, M.M. Haque, Titanium dioxide-mediated photocatalysed degradation of few selected organic pollutants in aqueous suspensions, *Catal. Today* 124 (2007) 133–148.
- [27] M.G. Neelavannan, M. Revathi, C. Ahmed Basha, Photocatalytic and electrochemical combined treatment of textile wash water, *J. Hazard. Mater.* 149 (2007) 371–378.
- [28] M.Y. Cheng, I.C. Yu, P.K. Wong, Degradation of azo dye Procion Red MX-5B by photocatalytic oxidation, *Chemosphere* 46 (2002) 905–912.